Mugla Journal of Science and Technology

AN EFFICIENT NUMERICAL SOLUTION METHOD FOR NONLINEAR KLEIN-GORDON EQUATION VIA TAYLOR WAVELET METHOD

Nurcan GÜCÜYENEN KAYMAK*, Department of Management Information Systems, Faculty of Economics and Administrative Sciences, Doğuş University, İstanbul, Turkey, nkaymak@dogus.edu.tr
(https://orcid.org/0000-0001-8226-8315)
Yeşim ÇİÇEK, Department of Engineering Sciences, Faculty of Engineering and Architecture, İzmir Katip Çelebi University, İzmir, Turkey, yesim.cicek@ikcu.edu.tr
(https://orcid.org/0000-0001-5438-4685)

Received: 02.07.2025, Accepted: 05.12.2025
Research Article
* Corresponding author
DOI: 10.22531/muglajsci.1733279

Abstract

The Klein–Gordon equation is of fundamental importance in mathematical physics, particularly due to its extensive applications in the analysis of solitonic phenomena, condensed matter systems, and the behavior of nonlinear wave dynamics. In this study, we develop a highly accurate numerical algorithm based on Taylor wavelets combined with the collocation technique, to approximate the solutions of nonlinear Klein-Gordon equations. An integration operational matrix is constructed and employed to transform the nonlinear Klein-Gordon initial–boundary value problem into an equivalent system of algebraic equations. One of the advantages of this method is that it does not require any restriction on domain discretization. This study also provides valuable insights into the underlying theoretical properties of the proposed method. To verify the reliability and accuracy of the proposed Taylor wavelet-based algorithm, a convergence analysis is performed. The method is then applied to four benchmark problems to further assess its effectiveness and computational performance. The comparison between the numerical and exact solutions demonstrates that the proposed method yields highly accurate results with minimal errors. All computations have been executed using MATLAB-2023b programming language.
Keywords: Numerical solution, Taylor Wavelet, Nonlinear wave, Error, Convergence

DOĞRUSAL OLMAYAN KLEIN–GORDON DENKLEMİ İÇİN TAYLOR DALGACIK YÖNTEMİYLE ETKİLİ BİR SAYISAL ÇÖZÜM YÖNTEMİ

Özet

Klein–Gordon denklemi, solitonik olayların analizi, yoğun madde sistemleri ve doğrusal olmayan dalga dinamiklerinin incelenmesi gibi geniş uygulama alanları nedeniyle matematiksel fizikte temel bir öneme sahiptir. Bu çalışmada, doğrusal olmayan Klein–Gordon denklemlerinin çözümlerini yaklaştırmak amacıyla Taylor dalgacıkları ile kolokasyon tekniğini birleştiren yüksek doğruluklu bir sayısal algoritma geliştirilmiştir. Oluşturulan integrasyon işlemsel matrisi, başlangıç–sınır değer problemindeki doğrusal olmayan Klein–Gordon denklemini eşdeğer bir cebirsel denklem sistemine dönüştürmek için kullanılmaktadır. Önerilen yöntemin önemli avantajlarından biri, tanım alanının ayrıklaştırılmasına yönelik herhangi bir kısıtlama gerektirmemesidir. Çalışma ayrıca yöntemin temelinde yer alan teorik özelliklere ilişkin değerli bilgiler sunmaktadır. Önerilen Taylor dalgacığı tabanlı algoritmanın doğruluğunu ve güvenilirliğini değerlendirmek amacıyla yakınsama analizi yapılmıştır. Yöntem daha sonra dört örnek problem üzerinde uygulanarak etkinliği ve hesaplama performansı test edilmiştir. Sayısal ve tam çözümlerin karşılaştırılması, yöntemin çok küçük hata değerleriyle yüksek doğruluk sağladığını göstermektedir. Tüm hesaplamalar MATLAB-2023b programlama ortamında gerçekleştirilmiştir.
Anahtar Kelimeler: Sayısal çözüm, Taylor Dalgacığı, Doğrusal olmayan dalga, Hata, Yakınsama

Cite

Kaymak, N. G., Çiçek, Y. (2025). "An Efficient Numerical Solution Method for Nonlinear Klein–Gordon Equation via Taylor Wavelet Method", Mugla Journal of Science and Technology, 11(2), 105-117.

1. Introduction

The Klein–Gordon equation plays a significant role in mathematical physics and has garnered considerable attention due to its applications in the study of solitons, condensed matter physics, and the dynamics of nonlinear wave equations. It is particularly relevant in analyzing soliton interactions in collision less plasma, exploring the recurrence of initial states, and investigating the broader behavior of nonlinear wave phenomena. The numerical investigation of the Klein–Gordon and sine-Gordon equations has received significant attention in recent

years. Several projection and numerical methods for the Klein–Gordon equation have been proposed in previous works, including those by [1] and [2]. Various analytical and numerical techniques are used in the approximations of Klein–Gordon equation both linear and nonlinear cases. In [3] homotopy analysis transform method is applied and the homotopy analysis is studied, Legendre wavelets are investigated in [4]. In the work [5] and [6], variational iteration method is applied for solving linear and nonlinear Klein–Gordon equations. Also, the results are compared with those obtained by Adomian's decomposition method. Variational homotopy perturbation method (VHPM) is employed to obtain approximate analytical solutions of the Klein–Gordon and sine-Gordon equations in [7] and the authors compare numerical results with the exact solutions, variational homotopy perturbation method (VHPM), modified Adomian decomposition method (MADM), [8], and variational iteration method [6]. In [9] , differential transform method for solving the linear and nonlinear Klein–Gordon equation is studied. In [10], the authors develop a new B-spline method for Klein-Gordon equations. In [11], the authors investigate approximate analytical solutions of both linear and nonlinear time-fractional Klein–Gordon equations using a recently developed semi-analytical technique known as the fractional reduced differential transform method (FRDTM). The method is applied under suitable initial conditions to effectively handle the fractional nature of the time derivative. In [12] they propose fast and high accuracy numerical methods for the solution of the one dimensional nonlinear Klein–Gordon equations. These methods are based on applying fourth order time-stepping schemes in combination with discrete Fourier transform to numerically solve the KG equations. In [13], multiquadric quasi-interpolation scheme and the integrated radial basis function are used to find numerical solution of the Klein-Gordon equations. In [14], the authors employed the Chebyshev wavelet approach to solve nonlinear Klein-Gordon and Sine-Gordon equations, demonstrating its ability to deliver accurate spatial and spectral results with efficient computation. In [15], exponent modified cubic B-spline differential quadrature method with the leave-one-out-cross-validation (LOOCV) approach is constructed for nonlinear Sine-Gordon equation.

Apart from all these methods mentioned above, Taylor wavelet method has got more attention of researcher from the last two decades, due to its features such as orthogonality, multi-resolution analysis, and computational efficiency. There are remarkable studies on Taylor wavelets for solving various types of equations. The following are a few notable instances: In [16], the efficiency of Taylor wavelet collocation method is demonstrated for the Benjamin-Bona-Mahony equation. In [17] generalized Burger-Huxley equation is studied using Taylor wavelet. Stiff systems in chemistry are studied via Taylor wavelet method in [18]. In [19], a novel approach under the Taylor wavelet and collocation is presented for HIV-infected CD4+T cells model. In [20], Taylor wavelet is studied for initial and boundary value problems of Bratu-type equations. In [21], general type of the KdV-Burger' Equation are solved numerically via Taylor wavelet method.

In this study, Taylor wavelet collocation algorithm is proposed for the numerical solution of the nonlinear Klein–Gordon equations. One of the key advantages of this method is that it operates without the need for spatial mesh generation, making it inherently mesh-free. Additionally, the method simplifies the problem by transforming the differential equation into a system of algebraic equations. It is also computationally efficient while maintaining a high level of accuracy. Beyond its numerical effectiveness, the study contributes to a deeper understanding of the theoretical properties associated with the proposed method.

In the present work, Klein-Gordon equations are considered in the form of,

$$\frac{\partial^2 u(x,t)}{\partial t^2} - \alpha^2 \frac{\partial^2 u(x,t)}{\partial x^2} + \frac{d\,V(u(x,t))}{du} = f(x,t), \qquad (1)$$

with initial conditions

$$u(x,0) = \eta_1(x), \quad \frac{\partial u(x,0)}{\partial t} = \eta_2(x), \quad x \in (a,b) \qquad (2)$$

and the boundary conditions

$$u(a,t) = \varphi_1(t), \quad u(b,t) = \varphi_2(t), \quad t \in [0,T] \qquad (3)$$

where α is a known constant, $\frac{d\,V(u(x,t))}{du}$ is a nonlinear function of u which is the derivative of potential energy V(u), η_1, η_2, φ_1 and φ_2 are real valued functions and f(x, t) is a real valued nonhomogenous term. During the paper, the potential energy function is taken into consideration as follows

$$V(u) = \frac{\beta_1}{2}u^2 + \frac{\beta_2}{3}u^3 + \cdots + \frac{\beta_n}{n+1}u^{n+1}, \qquad (4)$$

where $\beta_1, \beta_2, \ldots, \beta_n$ are real valued constants. One of the main characteristics of Equation (1) is that it conserves energy, [12]. The enery equation for Equation (1) is expressed as follows

$$E(t) = \frac{1}{2}\int [(u_t)^2 + \alpha^2 (u_x)^2 + 2V(u)]\,dx, \; x \in \mathbb{R}. \qquad (5)$$

The structure of the paper is organized as follows: Section 2 introduces the fundamental properties of Taylor wavelets and the algorithm of Taylor wavelet collocation method for KG equation is formulated. In Section 3, the convergence analysis of the proposed method is studied and also the numerical simulations of various nonlinear KG equations with varying potentials

are presented. Also the results are discussed. Finally, Section 4 concludes the study with a summary of the findings.

2. Materials and Methods

This section is devoted to explaining the application of Taylor wavelets to the nonlinear KG equation. To this end, Section 2.1 provides a detailed overview of the Taylor wavelets along with their integral representations. Following this, Section 2.2 outlines the numerical solution approach using these wavelets in a clear and systematic manner.

2.1. Introduction to Taylor wavelets

Wavelets are a set of functions derived by scaling and shifting a primary function referred to as the mother wavelet. Taylor wavelets, introduced by Keshavarz et al. [21], represent a significant class of wavelet-based numerical methods. Taylor wavelets, represented by ϕ_{pq}, on the interval [0,1) can be defined as follows

$$\phi_{pq}(x) = \begin{cases} 2^{\frac{k-1}{2}}\widehat{T}_q(2^{k-1}x - p + 1), & \frac{p-1}{2^{k-1}} \le x < \frac{p}{2^{k-1}} \\ 0, & \text{otherwise} \end{cases} \quad (6)$$

where $q = 0,1,2,\dots,M-1$, $p = 1,2,\dots,2^{k-1}$ and $\widehat{T}_q(x) = \sqrt{2q+1}x^q$ is a normalized Taylor polynomial of degree q. For example, the Taylor wavelets for the case $k = 1$ and $M = 6$ are given as

$$\{\phi_{10}(x), \phi_{11}(x), \phi_{12}(x), \phi_{13}(x), \phi_{14}(x), \phi_{15}(x)\} = \{1, \sqrt{3}x, \sqrt{5}x^2, \sqrt{7}x^3, \sqrt{9}x^4, \sqrt{11}x^5\}.$$

Therefore, any function, h(x), can be expressed in terms of Taylor wavelets as follows

$$h(x) = \sum_{p=1}^{\infty}\sum_{q=0}^{\infty} h_{pq}\phi_{pq}(x) \quad (7)$$

where h_{pq} represents the Taylor wavelet coefficients and are determined by $h_{pq} = < h(x), \phi_{pq}(x) >$ and $<,>$ is an inner product. By employing the truncated version of the infinite series in Equation (7), an approximation of h(x) can be formulated as follows

$$h(x) \cong \sum_{p=1}^{2^{k-1}}\sum_{q=0}^{M-1} h_{pq}\phi_{pq}(x) = H\Phi(x), \quad (8)$$

where

$$H = \begin{bmatrix} h_{10}, h_{11}, \dots, h_{1(M-1)}, h_{20}, h_{21}, \dots, h_{2(M-1)}, \dots, \\ h_{2^{k-1}0}, h_{2^{k-1}1}, \dots, h_{2^{k-1}(M-1)} \end{bmatrix}, \quad (9)$$

$$\Phi(x) = \begin{bmatrix} \phi_{10}(x), \dots, \phi_{1(M-1)}(x), \phi_{20}(x), \dots, \phi_{2(M-1)}(x), \\ \dots, \phi_{2^{k-1}0}(x), \dots, \phi_{2^{k-1}(M-1)}(x) \end{bmatrix}^T, \quad (10)$$

where H^T and $\Phi(x)$ are matrices with size of $M2^{k-1} \times 1$. The Taylor wavelets given in Equation (6) can be rewritten as follows

$$\phi_{pq}(x) = 2^{\frac{k-1}{2}}\sqrt{2q+1}(2^{k-1}x - p + 1)^q. \quad (11)$$

Assume that $P^m, m = 1,2$ is an integral operator. After integrating Equation (11) once with respect to x we get the following

$$P^1\phi_{pq}(x) = \int_0^x \phi_{pq}(x)\,dx = 2^{\frac{k-1}{2}}\sqrt{2q+1}\left(\frac{(2^{k-1}x-p+1)^{q+1}}{2^{k-1}(q+1)}\right). \quad (12)$$

After integrating Equation (11) twice with respect to x we get the following

$$P^2\phi_{pq}(x) = \int_0^x\int_0^x \phi_{pq}(x)\,dx\,dx = 2^{\frac{k-1}{2}}\sqrt{2q+1}\left(\frac{(2^{k-1}x-p+1)^{q+2}}{2^{2(k-1)}(q+1)(q+2)}\right). \quad (13)$$

After rearranging Equations (12) and (13), we obtain the generalized integral form of wavelets as follows

$$P^m\phi_{pq}(x) = \begin{cases} 0, & \text{if } 0 \le x < \frac{p-1}{2^{k-1}}; \\ \frac{2^{\left(q+\frac{1}{2}\right)(k-1)}q!\sqrt{2q+1}}{(q+m)!}\left(x - \frac{p-1}{2^{k-1}}\right)^{q+m}, & \text{if } \frac{p-1}{2^{k-1}} \le x < \frac{p}{2^{k-1}}; \\ \frac{2^{\left(q+\frac{1}{2}\right)(k-1)}q!\sqrt{2q+1}}{(q+m)!}\left(x - \frac{p-1}{2^{k-1}}\right)^{q+m} - R(x), & \text{if } \frac{p}{2^{k-1}} \le x \le 1, \end{cases} \quad (14)$$

where $m = 1,2$. Moreover,

$$R(x) = \sum_{j=1}^{q}\binom{q}{j}\frac{2^{\left(j+\frac{1}{2}\right)(k-1)}j!\sqrt{2q+1}}{(j+m)!}\left(x - \frac{p}{2^{k-1}}\right)^{j+m}. \quad (15)$$

See [21], [17], [20] for general references to Taylor wavelets and their integral forms.

2.2. Implementation of the method

This section is dedicated to explaining the proposed method in a clear and comprehensible manner. In order to apply the Taylor wavelet method to the equation defined in Equations (1)-(4), the physical domain [a, b] must first be mapped onto the interval [0, 1],see [22]. To do this, let $\chi = \frac{x-a}{L}$ where $L = a - b$. Following the transformation, Equations (1)-(4) are rewritten as follows:

$$\frac{\partial^2 y}{\partial t^2} - \frac{\alpha^2}{L^2}\frac{\partial^2 y}{\partial \chi^2} + \frac{dV(y)}{dy} = g(\chi, t), \chi \in (0,1), t > 0, \quad (16)$$

$$y(\chi,0)=\eta_1(\chi),\ \frac{\partial y(\chi,0)}{\partial t}=\eta_2(\chi),$$
$$y(0,t)=\varphi_1(t), y(1,t)=\varphi_2(t)$$

where $y(\chi,t)=u(x,t)$.

Based on the conditions imposed on the equation, the following relations can be derived:

$$\begin{aligned}&y(\chi,0)=\eta_1(\chi),\ y_\chi(\chi,0)=L\eta''_1(\chi),\ y_{\chi\chi}(\chi,0)=L^2\eta''_1(\chi),\\&y_t(\chi,0)=\eta_2(\chi), y_{t\chi\chi}(\chi,0)=L^2\eta''_2(\chi)\\&y(0,t)=\varphi_1(t),\ y_t(0,t)=\varphi'_1(t),\ y_{tt}(0,t)=\varphi''_1(t),\\&y(1,t)=\varphi_2(t), y_t(1,t)=\varphi'_2(t),\ y_{tt}(1,t)=\varphi''_2(t).\end{aligned}\quad(17)$$

Let the approximate solution be defined using the Taylor wavelet method as follows:

$$\frac{\partial^4 y(\chi,t)}{\partial t^2\,\partial\chi^2}=\sum_{p=1}^{2^{k-1}}\sum_{q=0}^{M-1}h_{pq}(t)\phi_{pq}(\chi)=H(t)\,\Phi(\chi).\quad(18)$$

Let $t_n=n\Delta t$ such that $\Delta t=T/N$, where N denotes the number of subdivisions within the time interval. In order to construct numerical solution, we start by integrating Equation (18) over $[t_n,t]$ with respect to t as follows

$$\int_{t_n}^{t}\frac{\partial^4 y(\chi,r)}{\partial t^2\,\partial\chi^2}\,dr\cong\int_{t_n}^{t}H(r)\Phi(\chi)\,dr,\ \text{where}\ t\in[t_n,t].\quad(19)$$

We assume that $Y(x,t)$ is the approximate solution. The function $H(r)$ is approximated via left-hand point and then Equation (19) yields the following

$$\frac{\partial^3 Y(\chi,t)}{\partial t\,\partial\chi^2}=(t-t_n)H(t_n)\Phi(\chi)+\frac{\partial^3 Y(\chi,t_n)}{\partial t\,\partial\chi^2},\quad(20)$$

where $t\in[t_n,t]$. Integrating Equation (20) over $[t_n,t]$ with respect to t yields the following:

$$\frac{\partial^2 Y(\chi,t)}{\partial\chi^2}=\frac{(t-t_n)^2}{2}H_n\Phi(\chi)+(t-t_n)\frac{\partial^3 Y(\chi,t_n)}{\partial t\,\partial\chi^2}+\frac{\partial^2 Y(\chi,t_n)}{\partial\chi^2}\quad(21)$$

where $H_n=H(t_n)$ for the sake of simplicity.

In order to find numerical solution $Y(\chi,t)$, we continue by integrating Equation (21) over $[0,x]$ with respect to x and this yields the followings

$$\frac{\partial Y(\chi,t)}{\partial\chi}=\frac{(t-t_r)^2}{2}H_nP^1\Phi(\chi)+(t-t_n)\left(\frac{\partial^2 Y(\chi,t_n)}{\partial t\,\partial\chi}-\frac{\partial^2 Y(0,t_n)}{\partial t\,\partial\chi}\right)+\left(\frac{\partial Y(\chi,t_n)}{\partial\chi}-\frac{\partial Y(0,t_n)}{\partial\chi}\right)+\frac{\partial Y(0,t)}{\partial\chi}.\quad(22)$$

Integrating Equation (21) once more over $[0,x]$ with respect to x yields the following:

$$Y(\chi,t)=\frac{(t-t_r)^2}{2}H_nP^2\Phi(\chi)+(t-t_n)\left(\frac{\partial Y(\chi,t_n)}{\partial t}-\frac{\partial Y(0,t_n)}{\partial t}-\chi\frac{\partial^2 Y(0,t_n)}{\partial t\,\partial\chi}\right)+\chi\left(\frac{\partial Y(0,t)}{\partial\chi}-\frac{\partial Y(0,t_n)}{\partial\chi}\right)+Y(\chi,t_n)+(Y(0,t)-Y(0,t_n)).\quad(23)$$

Here, $P^1\Phi(x)$, $P^2\Phi(x)$ are first and the second integrals of Taylor wavelets, respectively. It is important to note that every term in Equation (23) can be formulated using the initial and boundary conditions given in Equation (17) except for the term $\frac{\partial Y(0,t)}{\partial\chi}-\frac{\partial Y(0,t_n)}{\partial\chi}-(t-t_n)\frac{\partial^2 Y(0,t_n)}{\partial t\,\partial\chi}$, which remains independent. Accordingly, substituting $x=1$ into Equation (23) leads to the following expression:

$$\frac{\partial Y(0,t)}{\partial\chi}-\frac{\partial Y(0,t_n)}{\partial\chi}-(t-t_n)\frac{\partial^2 Y(0,t_n)}{\partial t\,\partial\chi}=Y(1,t)-\frac{(t-t_r)^2}{2}H_nP^2\Phi(1)-(t-t_n)\left(\frac{\partial Y(1,t_n)}{\partial t}-\frac{\partial Y(0,t_n)}{\partial t}\right)-Y(1,t_n)-\big(Y(0,t)-Y(0,t_n)\big).\quad(24)$$

After rearraging Equation (23), we get the following solution :

$$Y(\chi,t)=\frac{(t-t_n)^2}{2}H_n\big(P^2\Phi(\chi)-\chi P^2\Phi(1)\big)+(t-t_n)\left(\left(\frac{\partial Y(\chi,t_n)}{\partial t}-\frac{\partial Y(0,t_n)}{\partial t}\right)-\chi\left(\frac{\partial Y(1,t_n)}{\partial t}-\frac{\partial Y(0,t_n)}{\partial t}\right)\right)+\chi(Y(1,t)-Y(1,t_n))+(1-\chi)\big(Y(0,t)-Y(0,t_n)\big)+Y(\chi,t_n).\quad(25)$$

Furthermore, in order to complete algorithm, we need to calculate $\frac{\partial^2 Y}{\partial t^2}$. Taking the derivative of Equation (25) twice with respect to t leads to the following expression:

$$\frac{\partial^2 Y(\chi,t)}{\partial t^2}=H_n\big(P^2\Phi(\chi)-\chi P^2\Phi(1)\big)+\chi Y_{tt}(1,t)+(1-\chi)Y_{tt}(0,t).\quad(26)$$

Ultimately, by inserting Equations (21), (25) and (26) into the problem defined by Equation (16) at $t=t_{n+1}$, and utilizing the functions introduced in Equation (17), we arrive at the following numerical scheme

$$H_n\left(P^2\Phi(\chi)-\chi P^2\Phi(1)-\frac{\alpha^2\Delta t^2}{2L^2}\Phi(\chi)\right)=\frac{\alpha^2}{L^2}Y_{xx}(x,t_n)+\frac{\alpha^2\Delta t}{L^2}Y_{xxt}(x,t_n)-\chi\varphi''_2(t_{n+1})-(1-\chi)\varphi''_1(t_{n+1})-\frac{dV(Y)}{dY}+g(\chi,t).\quad(27)$$

It is clear that the right hand side of Equation (27) is known by the inital and boundary conditions given in Equation (17). By embedding the collocation points, $x_i=\frac{2i-1}{2^{k-1}M}$, $i=1,2,\dots,2^{k-1}M$ inside Equation (27), we obtain a system of equations. Then H_n is obtained after solving this system. Finally, we get the proposed numerical

solutions by substituting the obtained H_n inside Equation (25).

3. Results and Discussion

In this section, the convergence results of the proposed algorithm based on Taylor wavelet method and the numerical results are presented.

3.1. Convergence results

Convergence properties will be carried out in Theorem 3.3. It is important to highlight that all numerical results are computed using the ∞ norm to ensure a meaningful comparison with previous studies. Therefore, to maintain consistency throughout the manuscript, the convergence proof is also conducted within the framework of the L_∞ norm. To establish our main convergence result, we begin by presenting several supporting theorems.

Theorem 3.1. Let $h(x) \in \mathcal{C}^M[a,b]$. If $\mathcal{P}_M(x)$ interpolate $h(x)$ at the Chebyshev nodes over $[a,b]$, then by Theorem 4.5.5 in [22] the following inequality yields

$$\|h(x) - H\Phi(x)\|_\infty \leq \frac{2}{2^{M(k+1)}M!} \max_{\xi\in[0,1]} \left|h^{(M)}(\xi)\right|. \quad (28)$$

Theorem 3.2. Let $h(x) \in \mathcal{C}^M[0,1]$. Assume that $\sum_{p=1}^{2^{k-1}} \sum_{q=0}^{M-1} h_{pq}\Phi_{pq}(x) = H\Phi(x)$ is the best approximation of $h(x)$. Then, the error in the uniform norm satisfies the following bound:

$$\|h(x) - H\Phi(x)\|_\infty \leq \frac{2}{2^{M(k+1)}M!} \max_{\xi\in[0,1]} \left|h^{(M)}(\xi)\right| \quad (29)$$

and

$$\|P^n h(x) - HP^n\Phi(x)\|_\infty \leq \frac{2}{2^{M(k+1)}M!} \max_{\xi\in[0,1]} \left|h^{(M)}(\xi)\right| \quad (30)$$

where $n = 1, 2$. The proof of this theorem is given in details in [17].

Theorem 3.3. Assuming that $y: [0,1] \times [0, t_{end}] \to (a,b)$ is the exact solution of Equations (1)-(4) and $Y(x,t)$ represents the approximate solution. The proposed Taylor wavelet method is convergent such that

$$\|y(\chi, t_{n+1}) - Y(\chi, t_{n+1})\|_\infty \to 0$$

as k , M and N increase.

Proof. The numerical and the exact solution of the Equations (1)-(4) are defined as follows,

$$\begin{aligned} Y(\chi, t_{n+1}) = \frac{\Delta t^2}{2} \sum_{p=1}^{2^{k-1}} \sum_{q=0}^{M-1} H_n P^2 \Phi(\chi) + Y(\chi, t_n) \\ + \quad Y(0,t) - Y(0,t_n) \\ + \Delta t\left(Y_t(\chi, t_n) - Y_t(0,t_n)\right) \\ - \quad \Delta t\chi\left(Y_t(1,t_n) - Y_t(0,t_n)\right) \\ + \chi(Y(1,t) - Y(1,t_n) - Y(0,t) \\ + Y(0,t_n)) \end{aligned} \quad (31)$$

and

$$\begin{aligned} y(\chi, t_{n+1}) = \frac{\Delta t^2}{2} \sum_{p=1}^{\infty} \sum_{q=0}^{\infty} H_n P^2 \Phi(\chi) + y(\chi, t_n) \\ + \quad y(0,t) - y(0,t_n) \\ + \Delta t\left(y_t(\chi, t_n) - y_t(0,t_n)\right) \\ - \quad \Delta t\chi\left(y_t(1,t_n) - y_t(0,t_n)\right) \\ + \chi(y(1,t) - y(1,t_n) - y(0,t) \\ + y(0,t_n)) \end{aligned} \quad (32)$$

where $\Delta t = t_{n+1} - t_n$. Subtracting Equation (31) from Equation (32), then taking the infinity norm and using the triangle inequality yields the following:

$$\begin{aligned} \|e_{n+1}\|_\infty \leq \frac{\Delta t^2}{2} \Bigg\| \sum_{p=1}^{\infty} \sum_{q=0}^{\infty} H_n P^2 \Phi(\chi) \\ - \sum_{p=1}^{2^{k-1}} \sum_{q=0}^{M-1} H_n P^2 \Phi(\chi) \Bigg\|_\infty \\ + \frac{\Delta t^2}{2} \chi \Bigg\| \sum_{p=1}^{\infty} \sum_{q=0}^{\infty} H_n P^2 \Phi(1) \\ - \sum_{p=1}^{2^{k-1}} \sum_{q=0}^{M-1} H_n P^2 \Phi(1) \Bigg\|_\infty \\ + \|y(\chi, t_n) - Y(\chi, t_n)\|_\infty \\ + (1-\chi)\|y(0,t) - Y(0,t)\|_\infty \\ + +\varepsilon_1^{0,n} + \Delta t \left\| y_t(\chi, t_n) - Y_t(\chi, t_n) \right\|_\infty \\ + \Delta t\varepsilon_2^{0,n} + \Delta t\chi\left(\varepsilon_2^{1,n} + \varepsilon_2^{0,n}\right) \\ + \chi\|y(1,t) - Y(1,t)\|_\infty + \chi(\varepsilon_1^{1,n} \\ + \varepsilon_1^{0,n}) \end{aligned} \quad (33)$$

where $\varepsilon_1^{i,j} = \left\|y(i,t_j) - Y(i,t_j)\right\|_\infty$ and $\varepsilon_2^{i,j} = \|y_t(i,t_j) - Y_t(i,t_j)\|_\infty$ such that $\varepsilon_1^{i,j} = \varepsilon_2^{i,j} = 0$ for $i = 0,1$ and $j = n$ for all $n = 0,1,2,\ldots N$ and we assume that $\|y(\chi,t) - Y(\chi,t)\|_\infty$ and $\|y_t(\chi,t_n) - Y_t(\chi,t_n)\|_\infty$ are bounded for all χ values.

Then, Equation (33) can be written as follows

$$\|e_{n+1}\|_\infty \le \frac{\Delta t^2}{2}\left\| \sum_{p=1}^{\infty}\sum_{q=0}^{\infty} H_n P^2 \Phi(\chi) - \sum_{p=1}^{2^{k-1}}\sum_{q=0}^{M-1} H_n P^2 \Phi(\chi) \right\|_\infty + \frac{\Delta t^2}{2}\chi \left\| \sum_{p=1}^{\infty}\sum_{q=0}^{\infty} H_n P^2 \Phi(1) - \sum_{p=1}^{2^{k-1}}\sum_{q=0}^{M-1} H_n P^2 \Phi(1) \right\|_\infty + \|e_n\|_\infty. \quad (34)$$

As a result of the Theorem 3.2, we can conclude as follows

$$\|e_{n+1}\|_\infty \le \frac{\Delta t^2}{2^{M(k+1)} M!} \max_{\xi\in[0,1]} |h^M(\xi)| + \|e_n\|_\infty + \frac{\Delta t^2 \chi}{2^{M(k+1)} M!} \max_{\xi\in[0,1]} |h^M(1)| \quad (35)$$

As the parameters k, M and N increase, it follows that

$$\|e_{n+1}\|_\infty \le \|e_n\|_\infty. \quad (36)$$

Since Δt tends to zero as N grows the decreasing nature of the error sequence in Equation (36) by induction leads to

$$\|e_{n+1}\|_\infty \le \|e_0\|_\infty = 0. \quad (37)$$

3.2. Numerical results

The effectiveness of the developed algorithm is demonstrated through four different problems. The numerical results have been compared with the exact solutions and with the solutions from literature such as the multiquadric quasi-interpolation scheme (IMQQI), [13], modified Adomain decomposition method (MADM) [8], variational iteration method [6], [5], variational homotopy perturbation method [7], trigonometric function B-spline method [10], differential transform method [9].

The L_∞ L_2, Root Mean Square(RMS) error norms are defined as follows:

$$\|u(.,t_n) - Y(.,t_n)\|_{L_\infty} = \max_{1\le i\le N} |u(x_i,t_n) - Y(x_i,t_n)|,$$

$$\|u(.,t_n) - Y(.,t_n)\|_{L_2} = \sqrt{h\sum_{i=1}^{N}(u(x_i,t_n) - Y(x_i,t_n))^2},$$

$$RMS = \sqrt{\frac{1}{N+1}\sum_{i=1}^{N}(u(x_i,t_n) - Y(x_i,t_n))^2},$$

where $N = 2^{k-1}M$ and h is the space discretization number. Moreover, all numerical results will be obtained by collecting Newton-Codes nodes, $x_i = \frac{2i-1}{2^{k-1}M}$, $i = 1,2,\dots,2^{k-1}M$ with suitable k, M values. It should be noted that all computational results are obtained using MATLAB R2023b on a system equipped with an Intel Core i5 processor (1.00 GHz) and 8 GB of RAM.

Example 3.1 Consider the nonlinear KG Equations (1)-(4) with $\alpha = 1$, $n = 2$, $\beta_1 = 0$, $\beta_2 = 1$, $f(x,t) = 6xt(x^2 - t^2) + x^6t^6$ and the initial and the boundary conditions are given by

$$u(x,0) = 0,\ u_t(x,0) = 0, x \in (0,1), \quad u(0,t) = 0, u(1,t) = t^3, t \in [0,T]. \quad (38)$$

The exact solution is $u(x,t) = x^3t^3$, see [13].

To begin with, it is important to emphasize that when $k = 2$ and $M = 3$, the corresponding Taylor wavelet bases are given by:

$$\phi_{pq}(x) = \begin{cases} \sqrt{2}, & p=1,\ q=0,\ 0 \le x < \frac{1}{2}, \\ 2\sqrt{6}\,x, & p=1,\ q=1,\ 0 \le x < \frac{1}{2}, \\ 4\sqrt{10}\,x^2, & p=1,\ q=2,\ 0 \le x < \frac{1}{2}, \\ \sqrt{2}, & p=2,\ q=0,\ \frac{1}{2} \le x < 1, \\ \sqrt{6}\,(2x-1), & p=2,\ q=1,\ \frac{1}{2} \le x < 1, \\ \sqrt{10}\,(2x-1)^2, & p=2,\ q=2,\ \frac{1}{2} \le x < 1, \\ 0, & \text{otherwise.} \end{cases}$$

And the Taylor wavelet basis matrix, the second-order integration matrix and the second-order integration matrix evaluated at $x = 1$ are determined based on Equations (6) and (14), respectively, as presented below

$$\Phi_{6x6} = \begin{bmatrix} \sqrt{2} & \sqrt{2} & \sqrt{2} & 0 & 0 & 0 \\ 0.4081 & 1.2247 & 2.0414 & 0 & 0 & 0 \\ 0.0878 & 0.7906 & 2.1964 & 0 & 0 & 0 \\ 0 & 0 & 0 & \sqrt{2} & \sqrt{2} & \sqrt{2} \\ 0 & 0 & 0 & 0.4081 & 1.2247 & 2.0414 \\ 0 & 0 & 0 & 0.0878 & 0.7906 & 2.1964 \end{bmatrix}$$

$$P^2\Phi_{6x6} = \begin{bmatrix} 0.0049 & 0.0442 & 0.1228 & 0.2357 & 0.3536 & 0.4714 \\ 4.7194e-04 & 0.0128 & 0.0591 & 0.1531 & 0.2552 & 0.3572 \\ 5.0753e-05 & 0.0041 & 0.0318 & 0.1098 & 0.1976 & 0.2855 \\ 0 & 0 & 0 & 0.0049 & 0.0442 & 0.1228 \\ 0 & 0 & 0 & 4.7194e-04 & 0.0128 & 0.0591 \\ 0 & 0 & 0 & 5.0753e-04 & 0.0041 & 0.0318 \end{bmatrix}$$

$$P^2\Phi_{6x6}(1) = \begin{bmatrix} 0.5033 & 0.5033 & \cdots \\ 0.4088 & 0.4088 & \cdots \\ 0.3294 & 0.3294 & \cdots \\ 0.1768 & 0.1768 & \cdots \\ 0.1021 & 0.1021 & \cdots \\ 0.0659 & 0.0659 & \cdots \end{bmatrix}.$$

The solution is obtained by substituting these matrices into Equations (25)–(27) at each discretization point.

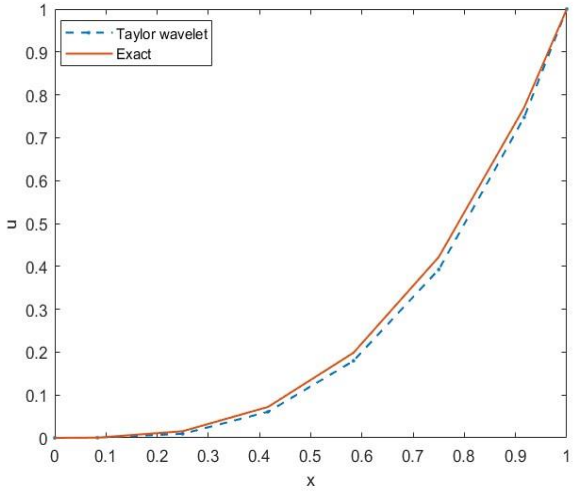

Figure 1. The Taylor wavelet and the exact solutions with $N = 6, \Delta t = 0.01$ at final time $T = 1$ for Example 3.1.

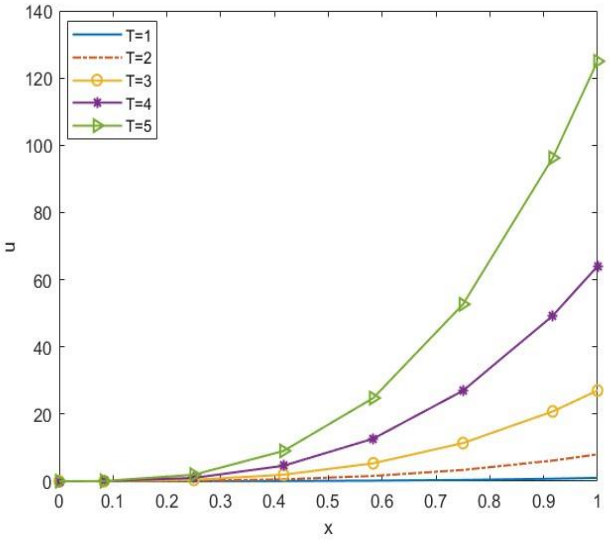

Figure 2. The Taylor wavelet solutions at different final times with $N = 6, \Delta t = 0.001$ for Example 3.1.

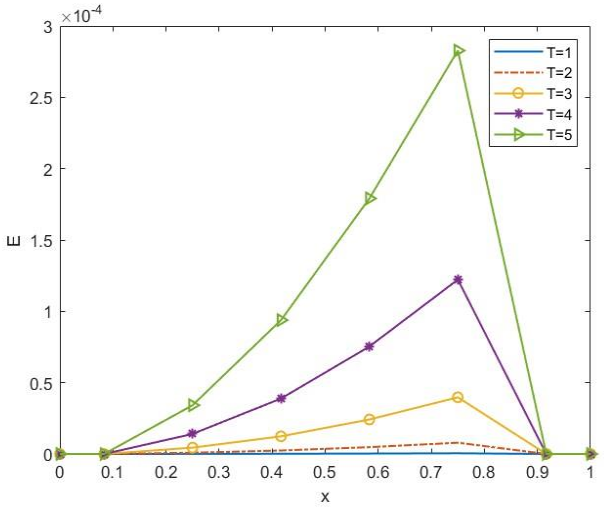

Figure 3. The L_2 errors of Taylor wavelet solutions at different times with $N = 6, \Delta t = 0.001$ for Example 3.1.

In Figure 1, the graphs of Taylor wavelet and the exact solutions of Example 3.1 with $N = 6(k = 2, M = 3), \Delta t = 0.01$ at final time $T = 1$ are presented. It is observed that both solutions are in good agreement with each other. In Figure 2 and Figure 3, the Taylor wavelet solutions and the L_2 errors of Taylor wavelet solutions at different final times are presented with $N = 6, \Delta t = 0.001$. The graphs exhibit similar behavior to those presented in [13], Experiment 1, Fig.1. In Table 1, L_∞ L_2, RMS errors, and corresponding CPU times are calculated at different final times with $N = 6, \Delta t = 0.0001$. Table 1 indicates that the Taylor wavelet method achieves comparable accuracy to the IMQQI method while requiring fewer spatial nodes. Moreover, the method maintains high accuracy with a low computational cost, and the CPU time exhibits a moderate increase with larger final times confirming the overall efficiency of the proposed algorithm.

Example 3.2 Consider the nonlinear KG Equations (1)-(4) with $\alpha = 1, n = 3, \beta_1 = 1, \beta_2 = 0, \beta_3 = 1$, $f(x,t) = (x^2 - 2)\cosh(x+t) - 4x\sinh(x+t) + x^6\cos^3 h(x+t)$ and the initial and the boundary conditions are given by

$$u(x,0) = x^2\cosh x,\ u_t(x,0) = x^2\sinh x, x \in (-1,1)$$
$$u(-1,t) = \cosh(-1+t),\ u(1,t) = \cosh(1+t), \quad (39)$$
$$t \in [0,T].$$

The exact solution is $u(x,t) = x^2\cosh(x+t)$, see [13].

To begin with, it is important to emphasize that when $k = 3$ and $M = 3$, the corresponding Taylor wavelet bases are given by:

$$\phi_{pq}(x) = \begin{cases} 2, & p=1,\ q=0,\ 0 \le x < \frac{1}{4}, \\ 2\sqrt{3}\,(4x), & p=1,\ q=1,\ 0 \le x < \frac{1}{4}, \\ 2\sqrt{5}\,(4x)^2, & p=1,\ q=2,\ 0 \le x < \frac{1}{4}, \\ 2, & p=2,\ q=0,\ \frac{1}{4} \le x < \frac{2}{4}, \\ 2\sqrt{3}\,(4x-1), & p=2,\ q=1,\ \frac{1}{4} \le x < \frac{2}{4}, \\ 2\sqrt{5}\,(4x-1)^2, & p=2,\ q=2,\ \frac{1}{4} \le x < \frac{2}{4}, \\ 2, & p=3,\ q=0,\ \frac{2}{4} \le x < \frac{3}{4}, \\ 2\sqrt{3}\,(4x-2), & p=3,\ q=1,\ \frac{2}{4} \le x < \frac{3}{4}, \\ 2\sqrt{5}\,(4x-2)^2, & p=3,\ q=2,\ \frac{2}{4} \le x < \frac{3}{4}, \\ 2, & p=4,\ q=0,\ \frac{3}{4} \le x < 1, \\ 2\sqrt{3}\,(4x-3), & p=4,\ q=1,\ \frac{3}{4} \le x < 1, \\ 2\sqrt{5}\,(4x-3)^2, & p=4,\ q=2,\ \frac{3}{4} \le x < 1, \\ 0, & \text{otherwise.} \end{cases}$$

And the Taylor wavelet basis matrix, the second-order integration matrix and the second-order integration matrix evaluated at x = 1 are determined based on Equations (6) and (14), respectively, as presented below.

The solution is obtained by substituting these matrices into Equations (25)–(27) at each discretization point.

The numerical simulations have been carried out by applying the proposed method to the transformed form of the equations, using suitably chosen approximate parameter values.

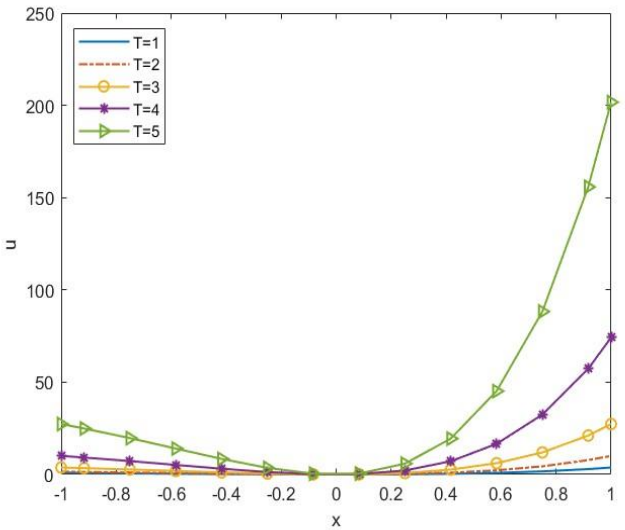

Figure 4. The Taylor wavelet solutions at different final times with N = 12, Δt = 0.001 for Example 3.2

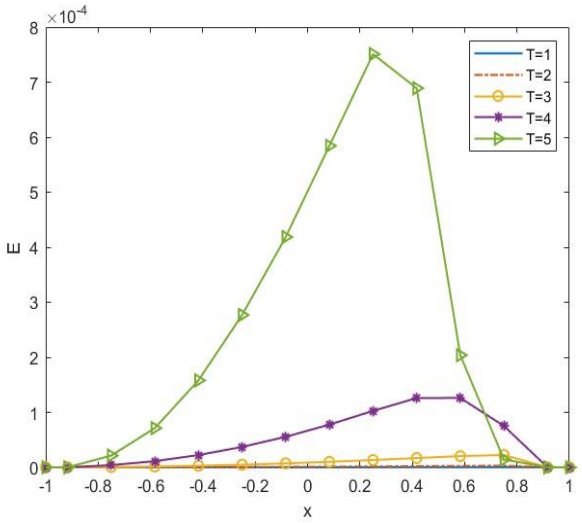

Figure 5. L_2 errors of Taylor wavelet solutions at different times with N = 12, Δt = 0.01 for Example 3.2.

$$P^2\Phi_{12\times12}(1) = \begin{bmatrix} 0.4375 & 0.4375 & \cdots \\ 0.3608 & 0.3608 & \cdots \\ 0.3028 & 0.3028 & \cdots \\ 0.3125 & 0.3125 & \cdots \\ 0.2526 & 0.2526 & \cdots \\ 0.2096 & 0.2096 & \cdots \\ 0.1875 & 0.1875 & \cdots \\ 0.1443 & 0.1443 & \cdots \\ 0.1165 & 0.1165 & \cdots \\ 0.0625 & 0.0625 & \cdots \\ 0.0361 & 0.0361 & \cdots \\ 0.0233 & 0.0233 & \end{bmatrix}$$

$$\Phi_{12\times12} = \begin{bmatrix}
2 & 2 & 2 & 0 & 0 & 0 & 0 & 0 & 0 & 0 & 0 & 0 \\
0.5778 & 1.7321 & 2.8863 & 0 & 0 & 0 & 0 & 0 & 0 & 0 & 0 & 0 \\
0.1244 & 1.118 & 3.1047 & 0 & 0 & 0 & 0 & 0 & 0 & 0 & 0 & 0 \\
0 & 0 & 0 & 2 & 2 & 2 & 0 & 0 & 0 & 0 & 0 & 0 \\
0 & 0 & 0 & 0.5778 & 1.7321 & 2.8863 & 0 & 0 & 0 & 0 & 0 & 0 \\
0 & 0 & 0 & 0.1244 & 1.118 & 3.1047 & 0 & 0 & 0 & 0 & 0 & 0 \\
0 & 0 & 0 & 0 & 0 & 0 & 2 & 2 & 2 & 0 & 0 & 0 \\
0 & 0 & 0 & 0 & 0 & 0 & 0.5778 & 1.7321 & 2.8863 & 0 & 0 & 0 \\
0 & 0 & 0 & 0 & 0 & 0 & 0.1244 & 1.118 & 3.1047 & 0 & 0 & 0 \\
0 & 0 & 0 & 0 & 0 & 0 & 0 & 0 & 0 & 2 & 2 & 2 \\
0 & 0 & 0 & 0 & 0 & 0 & 0 & 0 & 0 & 0.5778 & 1.7321 & 2.886 \\
0 & 0 & 0 & 0 & 0 & 0 & 0 & 0 & 0 & 0.1244 & 1.118 & 3.104
\end{bmatrix}$$

$$P^2\Phi_{12\times12} = \begin{bmatrix}
1.7e-03 & 0.015 & 0.043 & 0.083 & 0.125 & 0.116 & 0.208 & 0.25 & 0.201 & 0.333 & 0.375 & 0.416 \\
1.6e-04 & 0.004 & 0.020 & 0.054 & 0.090 & 0.126 & 0.162 & 0.198 & 0.234 & 0.278 & 0.306 & 0.342 \\
1.8e-05 & 0.001 & 0.011 & 0.038 & 0.069 & 0.1 & 0.132 & 0.163 & 0.194 & 0.225 & 0.256 & 0.287 \\
0 & 0 & 0 & 1.7e-03 & 0.015 & 0.043 & 0.083 & 0.125 & 0.116 & 0.208 & 0.25 & 0.291 \\
0 & 0 & 0 & 1.6e-4 & 0.004 & 0.020 & 0.054 & 0.090 & 0.126 & 0.162 & 0.198 & 0.234 \\
0 & 0 & 0 & 1.8e-5 & 0.001 & 0.011 & 0.038 & 0.069 & 0.1 & 0.132 & 0.163 & 0.194 \\
0 & 0 & 0 & 0 & 0 & 0 & 1.7e-03 & 0.015 & 0.043 & 0.083 & 0.125 & 0.116 \\
0 & 0 & 0 & 0 & 0 & 0 & 1.6e-04 & 0.004 & 0.020 & 0.054 & 0.090 & 0.126 \\
0 & 0 & 0 & 0 & 0 & 0 & 1.8e-05 & 0.001 & 0.011 & 0.038 & 0.069 & 0.1 \\
0 & 0 & 0 & 0 & 0 & 0 & 0 & 0 & 0 & 1.7e-03 & 0.015 & 0.04 \\
0 & 0 & 0 & 0 & 0 & 0 & 0 & 0 & 0 & 1.6e-04 & 0.004 & 0.02 \\
0 & 0 & 0 & 0 & 0 & 0 & 0 & 0 & 0 & 1.8e-05 & 0.001 & 0.011
\end{bmatrix}$$

In Figure 4 and Figure 5, the Taylor wavelet solutions and L_2 errors of Taylor wavelet solutions at different final times are presented with $N = 12(k = 3, M = 3)$, $\Delta t = 0.001$. The graphs exhibit similar behavior to those presented in [13], Experiment 3, Fig.3. In Table 2, L_∞ L_2, RMS errors, and the corresponding CPU times are calculated at different final times with $N = 12$, $\Delta t = 0.0001$. Table 2 indicates that the Taylor wavelet method achieves comparable accuracy to the IMQQI method [13] while requiring fewer spatial nodes. Moreover, the method maintains high accuracy with a low computational cost, and the CPU time exhibits a moderate increase with larger final times confirming the overall efficiency of the proposed algorithm.

Example 3.3 Consider the nonlinear Sine-Gordon equation as follows

$$\frac{\partial^2 u(x,t)}{\partial t^2} - \frac{\partial^2 u(x,t)}{\partial x^2} + \sin(u) = 0, \tag{40}$$

where $\alpha = 1$, $V(u) = -\cos u$, $f(x,t) = 0$ in Equations (1)-(4) and the initial conditions are given by

$$u(x,0) = 0, u_t(x,0) = 4\,\mathrm{sech}(x), x \in (0,1), \tag{41}$$

and the boundary conditions are obtained by the exact solution such that $u(x,t) = 4\tan^{-1}(t\,\mathrm{sech}(x))$, see [6], [8], [7].

In Table 3, the absolute errors of Taylor wavelet method at different times with $x = 0.1$, $N = 12$ are presented by comparing with the results in literature, such as 5-term of modified adomain decomposition method which is fourth order, [8], 2-iteration solution of variational iteration method which is second order, [6] and the 4-term of variational homotopy perturbation method which is third order, [7]. The Taylor wavelet method is second order when $M = 3$; thus, comparable accuracy is obtained with lower-degree polynomials. In Table 4, the comparison of the absolute errors between 3-term VHPM [7] which is second order and the Taylor wavelet method(TWM) at $x = 0.875$ with $N = 12$, $\Delta t = 0.01$ at various final times for Example 3.3 are presented. Moreover, the corresponding CPU times are presented. It can be observed that the absolute errors obtained by the Taylor wavelet method are smaller than those reported for other methods in the literature, which demonstrates the accuracy of the proposed approach. In Table 5, the L_∞ errors at various final times are compared with the results reported in [15], and the corresponding CPU times are also provided. It can be observed that the Taylor Wavelet Method (TWM) achieves comparable accuracy to the LOOCV method while using fewer spatial collocation points and maintaining smaller error values.

Considering Example 3.3 with space interval $-10 \le x \le 10$, Figure 6 illustrates the Taylor wavelet solutions at the final times $T = 1, 5, 10, 15, 20$, and for $\Delta t = 0.001$ and $N = 12$ $(k = 3, M = 3)$. The results indicate that the proposed method maintains good accuracy and stability even for large time intervals and relatively small matrix sizes. Furthermore, Figures 7(a) and 7(b) illustrate the corresponding surface plots of the Taylor wavelet and

the exact solutions at various time levels, with $\Delta t = 0.001$ and $N = 12$, highlighting the close agreement between the two. See [15], Figure 9, for comparison of the graphs.

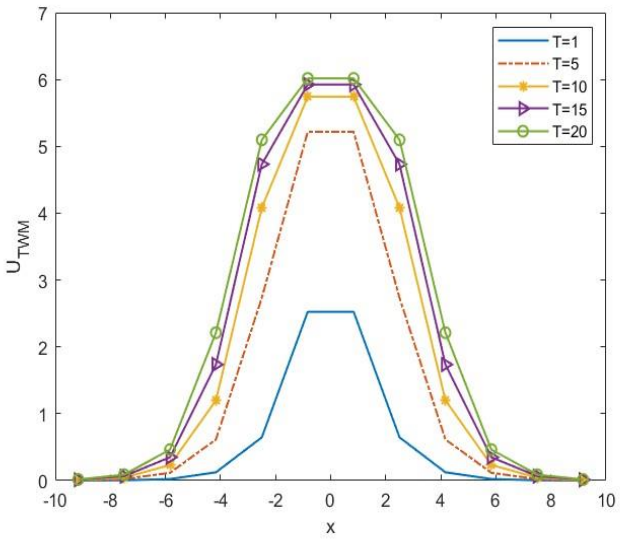

Figure 6. The Taylor wavelet solutions at different times with $N = 12, \Delta t = 0.001, -10 \le x \le 10$ for Example 3.3.

Example 3.4 Consider the nonlinear KG Equations (1)-(4) with $\alpha = 1, n = 2,\ \beta_1 = 0, \beta_2 = 1, f(x,t) = 0$ and the initial and the boundary conditions are given by

$$u(x,0) = 1 + \sin(x), u_t(x,0) = 0, x \in [0,1], \quad (41)$$
$$u(0,t) = 1 - \frac{t^2}{2}, u(1,t) = \frac{221}{120} - \frac{305t^2}{144} + \frac{103t^4}{144}, t \ge 0.$$

Since the exact solution is uknown, we compare our results with the other numerical approaches reported in literature, including the variational iteration method [5], the differential transform method [9] and the trigonometric function B-spline method [10]. Table 6 presents the numerical solutions at different times levels and at the spatial discretization points obtained using $N = 10$ ($k = 2, M = 5$) Taylor bases. The results indicate that the Taylor wavelet solutions exhibit behavior consistent with those of the existing methods in the literature. Here, the collocation points are selected as {0.1,0.2,0.3,0.4,0.5,0.6,0.7,0.8,0.9,1}. By substituting these points into Equations (6) and (14), the corresponding three Taylor matrices $(\Phi(\chi), P^2\Phi, P^2\Phi(1))$ are generated and subsequently used to construct the solution algorithms described in Equations (25), (27). The unknown terms given in (25)-(27) are $\frac{\partial u(\chi,t_{n+1})}{\partial t} = \frac{u(\chi,t_{n+1})-u(\chi,t_n)}{\Delta t}$, $\frac{\partial^3 u(\chi,t_{n+1})}{\partial t\,\partial\chi^2} = \Delta t H_n\Phi(\chi) + \frac{\partial^3 u(\chi,t_n)}{\partial t\,\partial\chi^2}$ and $\frac{\partial^2 u(\chi,t_{n+1})}{\partial\chi^2} = \frac{\Delta t^2}{2} H_n\Phi(\chi) + \Delta t \frac{\partial^3 u(\chi,t_n)}{\partial t\,\partial\chi^2} + \frac{\partial^2 u(\chi,t_n)}{\partial\chi^2}$ and they are calculated by taking the derivative of the given conditions such as $u_{txx}(x,t_0) = 0, u_{xx}(x,t_0) = -\cos(x), \quad u_{tt}(0,t_0) = -1, \quad u_{tt}(1,t_0) = -\frac{305}{72} + \frac{103}{12}t_0^2$ with $n = 0$.

Each H_n term is computed using Equation (27), and then substituted into Equation (25) to obtain Taylor wavelet solution.

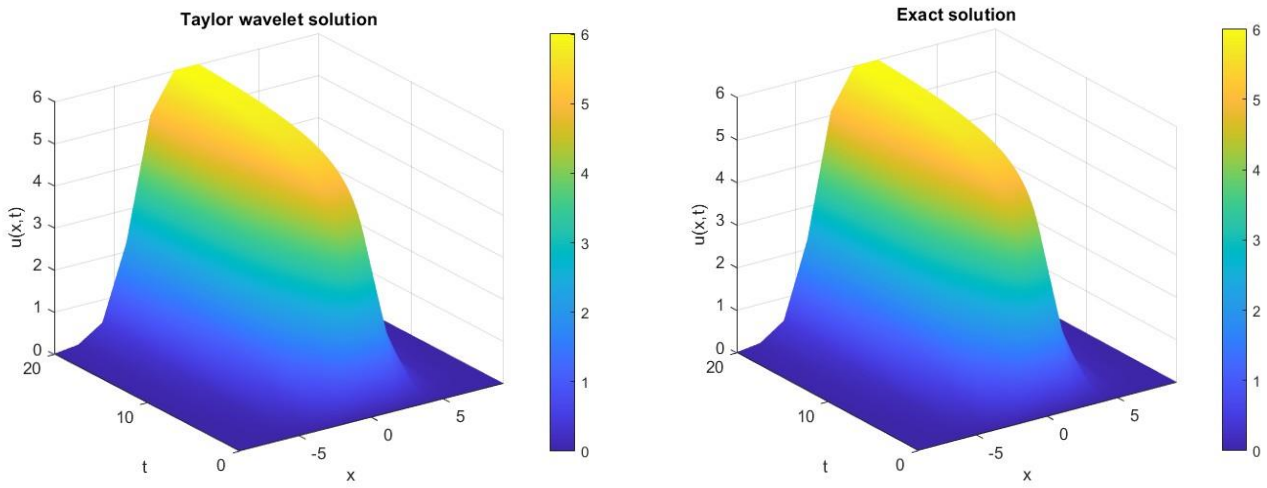

Figure 7.(a) The surface plot of the Taylor wavelet solutions for Example 3.3 over $0 \le t \le 20$. (b) The surface plot of the exact solutions.

Table 1. The comparison of various errors of Taylor wavelet method (TWM) with the results of [13] for Example 3.1.

T	TWM; N=6				IMQQI;N=20		
	L_∞	L_2	RMS	CPUtime(s)	L_∞	L_2	RMS
1	1.7325e-04	4.1094e-05	9.3174e-05	0.23174	7.7958e-06	3.4694e-05	4.8581e-06
2	6.9290e-04	4.0256e-04	3.7266e-04	0.41384	1.2307e-04	5.5475e-04	7.7680e-05
3	1.6000e-03	9.0540e-04	8.3816e-04	0.52633	5.3019e-04	2.4618e-03	2.4473e-04
4	2.8000e-03	1.6000e-03	1.5000e-03	0.69727	1.8601e-03	7.1623e-03	9.7029e-04
5	4.3000e-03	2.5000e-03	2.3000e-03	0.74830	3.5192e-03	1.3585e-02	1.9022e-03

Table 2. The comparison of various errors of Taylor wavelet method (TWM) with the results of [13] for Example 3.2.

T	TWM; N=12				IMQQI;N=50		
	L_∞	L_2	RMS	CPUtime(s)	L_∞	L_2	RMS
1	1.6717e-04	9.6681e-05	9.2907e-05	0.31663	4.2672e-05	2.8456e-04	2.0242e-05
2	5.9929e-04	3.4678e-04	3.3324e-04	0.47550	4.9397e-04	2.6266e-03	1.8577e-04
3	1.8000e-03	1.0000e-03	9.8027e-04	0.67779	2.0380e-03	9.5859e-03	6.7016e-04
4	4.7000e-03	2.8000e-03	2.7000e-03	0.78864	6.4162e-03	2.3457e-02	1.8844e-03
5	1,1100e-02	7.1000e-03	6.8000e-03	0.94703	1.7941e-02	7.4214e-02	5.2391e-03

Table 3. The comparison of the absolute errors between 5-term MADM [8], 2-iterate VIM [6], 4-term VHPM [7] and Taylor wavelet method (TWM) at $x = 0.1$ for Example 3.3.

T	|Exact-TWM|	|Exact-MADM|	|Exact-VIM|	|Exact-VHPM|
0.01	1.655×10^{-6}	1.925×10^{-4}	4.974×10^{-7}	5.007×10^{-8}
0.02	2.963×10^{-6}	3.926×10^{-4}	3.978×10^{-6}	4.003×10^{-7}
0.03	3.922×10^{-6}	6.079×10^{-4}	1.341×10^{-5}	1.350×10^{-6}
0.04	4.524×10^{-6}	8.453×10^{-4}	3.176×10^{-5}	3.195×10^{-6}
0.05	4.764×10^{-6}	1.112×10^{-3}	6.195×10^{-5}	6.229×10^{-6}
0.06	4.630×10^{-6}	1.413×10^{-3}	1.069×10^{-4}	1.074×10^{-5}
0.07	4.113×10^{-6}	1.757×10^{-3}	1.694×10^{-4}	1.701×10^{-5}
0.08	3.197×10^{-6}	2.147×10^{-3}	2.523×10^{-4}	2.531×10^{-5}
0.09	1.867×10^{-6}	2.591×10^{-3}	3.583×10^{-4}	3.592×10^{-5}
0.1	1.069×10^{-7}	3.092×10^{-3}	4.901×10^{-4}	4.909×10^{-5}

Table 4. The comparison of the absolute errors between 3-term VHPM [7] and the Taylor wavelet method (TWM) at $x = 0.875$ with $N = 12$ for Example 3.3.

T	|Exact-TWM|	CPU time(s)	|Exact-VHPM|
0.02	5.0760e-06	0.02647	7.6437e-06
0.04	1.7770e-05	0.03391	6.1121e-05
0.06	3.8601e-05	0.03482	2.0613e-04
0.08	6.5920e-05	0.04077	4.8810e-04
0.1	1.0131e-04	0.04485	9.5211e-04
0.2	3.8910e-04	0.05097	0.0076
0.3	8.5382e-04	0.06886	0.0255

Table 5. The comparison of L_∞ errors at different times for Example 3.3.

$\Delta t = 0.01$	TWM (N=12)	CPU time(s)	LOOCV, [15] (N=25)
T=1	1.5e-03	0.044541	1.65e-02
T=2	6.9e-03	0.057098	1.85e-02
T=5	2.45e-02	0.060838	1.66e-02
$\Delta t = 0.001$			
T=1	1.481e-04	0.097685	--
T=2	6.9473e-04	0.097401	--
T=5	2.5e-03	0.123591	--

Table 6. The comparison of the solutions for various numerical methods at different points for Example 3.4.

	x	0.1	0.2	0.4	0.6	0.8	1
T=0.1	[10]	1.09329	1.19050	1.37784	1.54957	1.69872	1.82056
	[9]	1.09333	1.19060	1.37807	1.55000	1.69908	1.82120
	[5]	1.09329	1.19050	1.37784	1.54962	1.69908	1.82038
	TWM	1.09294	1.18059	1.37040	1.54469	1.69663	1.82055
T=0.2	[10]	1.07373	1.16613	1.34340	1.50516	1.64498	1.75809
	[9]	1.07372	1.16613	1.34342	1.50505	1.64467	1.75808
	[5]	1.07372	1.16613	1.34343	1.50507	1.64499	1.75808
	TWM	1.07231	1.14562	1.33143	1.50484	1.65242	1.75808
T=0.3	[10]	1.04132	1.12598	1.28712	1.43198	1.55749	1.65684
	[9]	1.04131	1.12597	1.28708	1.43244	1.55706	1.65683
	[5]	1.04132	1.12597	1.28708	1.43249	1.55721	1.65720
	TWM	1.03826	1.09486	1.27334	1.44540	1.57711	1.65683

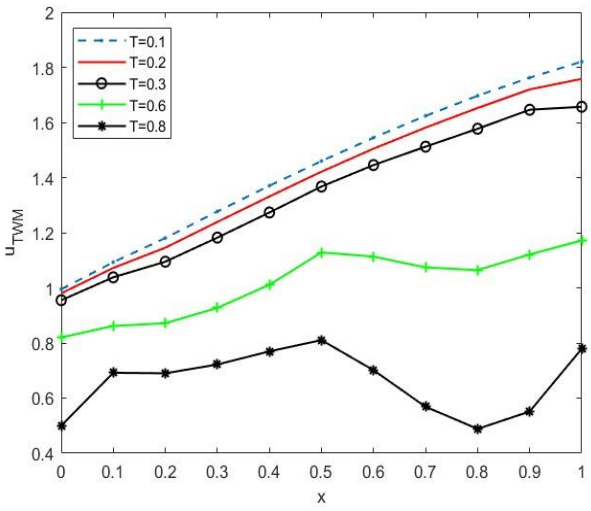

Figure 8. The Taylor wavelet solutions at different times with $N = 10$, over $0 \leq x \leq 1$ for Example 3.4.

In Figure 8, the Taylor wavelet solutions at different times with $N = 10(k = 2, M = 5)$ are simulated for Example 3.4.

4. Conclusion

This study primarily introduces a numerical technique utilizing the Taylor wavelet method to solve the nonlinear Klein-Gordon equations. A thorough theoretical analysis of the method has been conducted; a detailed convergence analysis has been carried out to validate the effectiveness of the approach. The method's accuracy has also been confirmed through numerical experiments on benchmark problems. The numerical experiments demonstrate that TWM provides accurate and stable solutions even for large time intervals and relatively small matrix sizes. A significant advantage of the present approach lies in its mesh-free structure, which eliminates the need for complex meshing or domain partitioning. Consequently, the implementation becomes simpler and computationally less expensive. The reported CPU times also confirm the computational efficiency of TWM.

Moreover, the method achieves high accuracy with a small number of collocation nodes, highlighting its spectral-like convergence and suitability for problems requiring fine spatial resolution. The accompanying tables and figures illustrate a strong agreement between the numerical and the exact solutions. The comparison of the numerical results with the exact solutions and with the methods in literature confirms that the proposed method achieves remarkable accuracy.

In summary, the Taylor Wavelet Collocation Method offers a robust, efficient, and accurate framework for solving nonlinear partial differential equations. Owing to its flexibility and performance, the method can be readily extended to higher-dimensional or fractional-order problems, making it a promising tool for future applications in scientific and engineering computations.

5. References

[1] Lynch, M. A. M., "Large Amplitude Instability in Finite Difference Approximations to the Klein-Gordon Equation", *Applied Numerical Mathematics,* 31(2), 173-182, 1999.

[2] Hariharan, G., "Haar Wavelet Method for Solving Klein–Gordon and Sine–Gordon Equations", *International Journal of Nonlinear Sciences,* 11(2), 180-189, 2011.

[3] Kumar, D., Singh, J., Kumar, S. and Sushila, S., "Numerical Computation of Klein–Gordon Equations Arising in Quantum Field Theory by Using Homotopy Analysis Transform Method", *Alexandria Engineering Journal,* 53(2), 469-474, 2014.

[4] Hesameddini, E. and Shekarpaz, S., "Wavelet Solutions of Klein-Gordon Equation", *Journal of Mahani Mathematical Research,* 1(1), 29-45, 2012.

[5] Yusufoğlu, E., "The Variational Iteration Method for Studying the Klein-Gordon Equation", *Applied Mathematics Letters,* 21(7), 669-674, 2008.

[6] Batiha, B., Noorani, M. S. and Hashim, I., "Numerical Solution of Sine-Gordon Equation by Variational Iteration Method", *Physics Letters A,* 370(5-6), 437-440, 2007.

[7] Yousif, M. A. and Mahmood, B. A., "Approximate Solutions for Solving the Klein-Gordon and Sine-Gordon Equations", *Journal of the Association of Arab Universities for Basic and Applied Sciences,* 22, 83-90, 2017.

[8] Kaya, D., "A Numerical Solution of the Sine-Gordon Equation Using the Modified Decomposition Method", *Applied Mathematics and Computation,* 143, 309–317, 2003.

[9] Kanth, A. R. and Aruna, K., "Differential Transform Method for Solving the Linear and Nonlinear Klein–Gordon Equation", *Computer Physics Communications,* 180(5), 708-711, 2009.

[10] Zadvan, H. and Rashidina, J., "Development of Non-Polynomial Spline and New B-spline with Application to Solution of Klein–Gordon Equation", *Computational Methods for Differential Equations,* 8(4), 794–814, 2020.

[11] Tamsir M. and Srivastava, V. K., "Analytical Study of Time-fractional Order Klein-Gordon Equation", *Alexandria Engineering Journal,* 55(1), 561-567, 2016.

[12] Mohebbi, A., Asgari Z. and Shahrezaee, A., "Fast and High Accuracy Numerical Methods for the Solution of Nonlinear Klein–Gordon Equations", *Zeitschrift für Naturforschung A,* 66(12), 735-744, 2011.

[13] Sarboland, M. and Aminataei, A., "Numerical Solution of the Nonlinear Klein-Gordon Equation Using Multiquadric Quasi-interpolation Scheme", *Universal journal of Applied Mathematics,* 3(3), 40-49, 2015.

[14] Rustam, A. and Javid, I., "Numerical Solution of Klein/Sine-Gordon Equations by Spectral Method Coupled with Chebyshev Wavelets", *Applied Mathematics,* 7(17), 2097-2109, 2016.

[15] Rani, R., Arora, G. and Bala, K., "Numerical Solution of One-dimensional Nonlinear Sine–Gordon Equation Using LOOCV with Exponential B-spline", *Computational and Applied Mathematics,* 43(4), 1-19, 2024.

[16] Shiralashetti, S. C. and Hanaji, S. I., "Taylor Wavelet Collocation Method for Benjamin-Bona-Mahony Partial Differential Equations", *Results in Applied Mathematics,* 9, 100139, 2021.

[17] Korkut, S. Ö., "An Accurate and Efficient Numerical Solution for the Generalized Burgers–Huxley Equation via Taylor Wavelets Method: Qualitative Analyses and Application", *Mathematics and Computers in Simulation,* 209(2023), 324–341, 2023.

[18] Manohara, G. and Kumbinarasaiah, S., "Numerical Solution of Some Stiff Systems Arising in Chemistry via Taylor Wavelet Collocation Method", *Journal of Mathematical Chemistry*, 62, 24–61, 2024.

[19] Vivek, Kumar, M. and Mishra, S. N., "A Fast Taylor-Wavelet Based Numerical Algorithm for the Solution of HIV-infected CD4+T Cells Model", *Filomat,* 38(8), 2949–2963, 2024.

[20] Korkut, S. Ö. and Karabaş, N. İ., "A Reliable Explicit Method to Approximate the General Type of the KdV-Burger' Equation", *Iranian Journal of Science and Technology, Transactions A: Science,* 46, 239-249, 2022.

[21] Keshavarza, E., Ordokhania, Y. and Razzaghi, M., "The Taylor Wavelets Method for Solving the Initial and Boundary Value Problems of Bratu-type Equations", *Appl. Numer. Math.,* 128, 205-216, 2018.

[22] Dahlquist, G. and Björck, Å., *Numerical Methods in Scientific Computing*, Stokholm: Society for Industrial and Applied Mathematics, 2008.